Michigan State University

PROPERTIES OF THE PHI MESON AT FINITE TEMPERATURE

KEVIN L. HAGLIN and CHARLES GALE
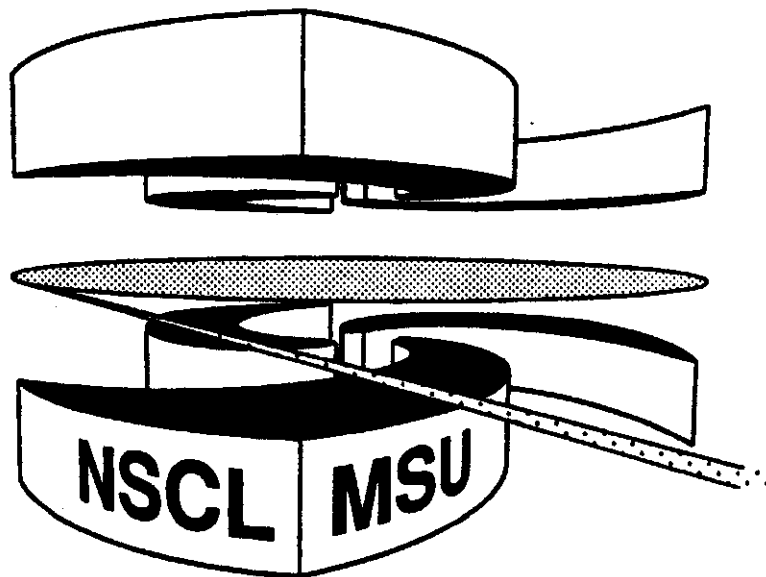
Properties of the phi meson at finite temperature

Kevin L. Haglin*

Notional Superconducting Cyclotron *Laboratory,* Michigan *State University*
East Lansing, Michigan *48824–1321*

Charles Gale**

Physics Department, McGill University, *3600 University Street*
Montréal, QC H3A 2T8, Canada
(May 26, 1994)

Abstract

We calculate the ϕ-meson propagator at finite temperature at the one-loop order. The real and imaginary parts are studied separately in full kinematic ranges. From this activity we investigate how temperature affects such things as decay widths and dispersion relations. Prom here we estimate the thermal rate of lepton pair radiation in a hadron gas proceeding through $K^+ K^- \rightarrow \phi \rightarrow \ell^+\ell^-$ and $\pi\rho \rightarrow \phi \rightarrow \ell^+\ell^-$. We find several interesting things. Prom the dispersion relations we learn the effective mass calculated this way increases with temperature as does the partial width, but only slightly. At $T = 200$ MeV, the mass increases by ~ 4 MeV and the partial width increases by 23%. Polarizations are indistinguishable for practical purposes.

PACS numbers: 25.75.+r, 12.38.Mh, 13.75.Lb

Typeset using REVTEX

I. INTRODUCTION

Attention is focused nowadays on problems relating to the physics of ultra-relativistic heavy-ion collisions where the primary purpose is to establish whether or not one can make a quark-gluon plasma (QGP). Regardless of the outcome of this query, the hadronic phase is present and it behooves us to continue thought and calculation regarding hadronic mechanisms in this extremely hot environment. It is clear that hadronic properties are modified at finite temperature. But to what extent such modifications are noticeable and for which hadrons this becomes important is not so easy to say. By studying these modifications we may be able to better understand what is happening as temperatures approach that which is expected to give a phase transition to the chirally symmetric QGP phase. There have been several studies of meson masses at finite temperature. Some employ lattice QCD (quantum chromodynamic) methods [1,2], and others use QCD sum rules [3,4]. Still others have used effective Lagrangian methods [5,6]. Our choice is the latter which uses finite-temperature field theory.

There are more than a half dozen hadrons with masses less then ~ 1 GeV. At the upper end of that range sits the ϕ-meson. It is a well known two-kaon resonance that is less abundant in these heavy-ion collisions than ρs or their decay products, the pions. On the other hand, the invariant mass distribution of lepton pairs is expected to show a noticeable structure near the ϕ's peak [7] so it is important at some level. Its finite temperature behavior including two-kaon annihilation into lepton pairs has been studied [5]. Deviation from vacuum behavior was concluded to be quite small. Yet, this was in some sense not surprising since the kaons are 3–4 times more massive than temperatures of interest. Again, the ϕ-meson decays into two kaons with highest rate but only somewhat less often decays into a $\pi\rho$ combination. The combined mass of the $\pi\rho$ system is smaller than the two-kaon threshold but not by enough to argue that the rate is sizeable merely due to phase space. The pion in the $\pi\rho$ decay of the ϕ might be more strongly affected by temperature than the kaons since it much less massive. Of course, the opposite argument applies to the ρ being more massive than the kaons, so a priori it is not clear what will happen to the whole system. The questions we attempt to answer are the following. How does the $\pi\rho$ decay possibility affect the ϕ's zero and finite temperature behavior? And, how does it affect the dispersion relation, i.e. does the effective mass remain the same, go up or down? The interesting role played by ϕ mesons and their lepton pair decay channel has previously been pointed out in the context of high energy heavy ion collisions [8].

Our paper is organized in the following way. In Sec. II we briefly discuss the one-loop kaon diagrams' contributions to the ϕ self-energy. They have been computed and appear in the literature [5]. We then evaluate the $\pi\rho$ loop's contribution and add it to the kaon diagrams. With all these, we have an improved ϕ-meson self-energy. It is a simple task to get from their to the full propagator which we present in Sec. III. Many properties of the resonance are contained within the propagator. Among them, we present effective widths and masses and dispersion relations. We finish with a short discussion on the thermal dilepton emission rates which are evaluated from knowledge of the finite temperature behavior of the imaginary part of the propagator. Finally, in Sec. IV we summarize and conclude that temperature effects are quite modest in this improved ϕ-meson propagator.

2

II. ϕ-MESON SELF-ENERGY TO ONE-LOOP

Vector mesons interact in a renormalizable fashion with a conserved current. The full Lagrangian for K-ϕ dynamics is

$$\mathcal{L} = \frac{1}{2}|D_\mu K|^2 - \frac{1}{2}m_K^2|K|^2 - \frac{1}{4}\phi_{\mu\nu}\phi^{\mu\nu} + \frac{1}{2}m_\phi^2\phi_\mu\phi^\mu, \tag{2.1}$$

where K is the complex charged kaon field, $\phi_{\mu\nu} = \partial_\mu\phi_\nu - \partial_\nu\phi_\mu$ is the ϕ field strength tensor, and $D_\mu = \partial_\mu - ig_{\phi KK}\phi_\mu$ is the covariant derivative. This gives rise to two diagrams which contribute to the self-energy at the one-loop level shown in Figs. 1a and 1b. We go further by including a ϕ-ρ-π interaction given by the Lagrangian [9]

$$\mathcal{L}_{\rm int} = g_{\phi\rho\pi}\epsilon_{\mu\nu\alpha\beta}\partial^\mu\phi^\nu\partial^\alpha\rho^\beta \cdot \boldsymbol{\pi}, \tag{2.2}$$

where the complex charged rho and pion fields appears as ρ^β and $\boldsymbol{\pi}$. This term gives the diagram shown in Fig. 1c. The kaon bubble and tadpole diagrams have been evaluated (by one of us along with J. Kapusta) and appear in the literature [5]. So we discuss only the $\pi\rho$ loop diagram. Its contribution to the self-energy in Euclidean space is

$$\Pi^{\mu\nu}(k) = 3g_{\phi\rho\pi}^2 \, T\sum_{p_4} \int \frac{d^3p}{(2\pi)^3} \frac{\mathcal{I}^{\mu\nu}}{(p^2 + m_\pi^2)\left[(p+k)^2 + m_\rho^2\right]} \tag{2.3}$$

where

$$\mathcal{I}^{\mu\nu} = [(k\cdot p)^2 - p^2k^2]\delta^{\mu\nu} + p^2k^\mu k^\nu + k^2p^\mu p^\nu - (k\cdot p)[p^\mu k^\nu + k^\mu p^\nu]. \tag{2.4}$$

The factor of 3 accounts for a sum over loop isospin. In the imaginary-time formalism, the indices run not from 0 to 3 but 1 to 4. The fourth component of the four-vectors are Matsubara frequencies, p_4 and $k_4 = 2\pi T \times$ integer.

As with all imaginary-time calculations, the zero temperature piece naturally separates from the T dependent piece. We have evaluated the expression in Eqs. (2.3) and (2.4) at $T = 0$ using dimensional regularization [10]. The rest, which depends on temperature, is obtained by converting the discrete sum over frequencies to a contour integral. We find it convenient to present the zero temperature results separately. For this π-ρ loop we obtain

$$\begin{aligned}
\Pi_{\rm vac}^{\mu\nu}(k) = \frac{g_{\phi\rho\pi}^2}{16\pi^2}\Big(k^\mu k^\nu - k^2\delta^{\mu\nu}\Big)\Bigg\{ &\frac{1}{4k^2}\Big((m_\rho^2 - m_\pi^2 + k^2)^2 + 4m_\pi^2 k^2\Big)\sqrt{\mathcal{R}} \\
&\times \ln\frac{\left(1 + \frac{m_\rho^2-m_\pi^2}{k^2} + \sqrt{\mathcal{R}}\right)\left(1 - \frac{m_\rho^2-m_\pi^2}{k^2} + \sqrt{\mathcal{R}}\right)}{\left(1 + \frac{m_\rho^2-m_\pi^2}{k^2} - \sqrt{\mathcal{R}}\right)\left(1 - \frac{m_\rho^2-m_\pi^2}{k^2} - \sqrt{\mathcal{R}}\right)} \\
&- \frac{1}{2k^4}(m_\rho^2 - m_\pi^2 + k^2)\left[\left(m_\rho^2 - m_\pi^2 + k^2\right)^2 + 6m_\pi^2 k^2\right]\ln\left(\frac{m_\rho}{m_\pi}\right) \\
&- \frac{5}{6}k^2 - \frac{(m_\rho^2 - m_\pi^2)^2}{2k^2} - 2\left(m_\rho^2 + m_\pi^2\right) + C\left(3m_\rho^2 + 3m_\pi^2 + k^2\right)\Bigg\} \tag{2.5}
\end{aligned}$$

at $T = 0$, with

3

$$\mathcal{R} = \left(1 + \frac{m_\rho^2 - m_\pi^2}{k^2}\right)^2 + \frac{4m_\pi^2}{k^2}, \tag{2.6}$$

and where C is a renormalization constant to be determined later. Then at $T > 0$

$$\begin{aligned}
\Pi_{\text{mat}}^{44}(k) = 3\left(\frac{g_{\phi\rho\pi}}{2\pi}\right)^2 \int_0^\infty dp\, p^2 \Bigg\{ &\frac{1}{\omega_\pi}\Bigg[\frac{-(k_4^2 + \mathbf{k}^2 + m_\rho^2 - m_\pi^2)}{2} \\
&+ \frac{4\omega_\pi^2 k_4^2 + 4p^2\mathbf{k}^2 - (k_4^2 + \mathbf{k}^2 + m_\rho^2 - m_\pi^2)^2}{16p|\mathbf{k}|}\ln a_\pi \\
&+ \frac{i\omega_\pi k_4(k_4^2 + \mathbf{k}^2 + m_\rho^2 - m_\pi^2)}{4p|\mathbf{k}|}\ln b_\pi\Bigg]\frac{1}{e^{\beta\omega_\pi} - 1} \\
&+ \frac{1}{\omega_\rho}\Bigg[\frac{-(k_4^2 + \mathbf{k}^2 + m_\pi^2 - m_\rho^2)}{2} \\
&+ \frac{4\omega_\rho^2 k_4^2 + 4p^2\mathbf{k}^2 - (k_4^2 + \mathbf{k}^2 + m_\pi^2 - m_\rho^2)^2}{16p|\mathbf{k}|}\ln a_\rho \\
&+ \frac{i\omega_\rho k_4(k_4^2 + \mathbf{k}^2 + m_\pi^2 - m_\rho^2)}{4p|\mathbf{k}|}\ln b_\rho\Bigg]\frac{1}{e^{\beta\omega_\rho} - 1}\Bigg\}, \tag{2.7}
\end{aligned}$$

$$\Pi_{\text{mat}}^{4i}(k) = -\frac{k_4 k^i}{\mathbf{k}^2}\Pi_{\text{mat}}^{44}(k), \tag{2.8}$$

and

$$\Pi_{\text{mat}}^{ij}(k) = A\delta^{ij} + \frac{k^i k^j}{\mathbf{k}^2}B \tag{2.9}$$

where

$$\begin{aligned}
A = 3\left(\frac{g_{\phi\rho\pi}}{2\pi}\right)^2 \int_0^\infty dp\, p^2 \Bigg\{ &\frac{1}{\omega_\pi}\Bigg[\frac{(k_4^2 - \mathbf{k}^2)(k_4^2 + \mathbf{k}^2 + m_\rho^2 - m_\pi^2)}{4\mathbf{k}^2} \\
&+ \left(\frac{(k_4^2 - \mathbf{k}^2)\left((k_4^2 + \mathbf{k}^2 + m_\rho^2 - m_\pi^2)^2 - 4\omega_\pi^2 k_4^2\right)}{32p|\mathbf{k}|^3} - \frac{\omega_\pi^2 k_4^2}{2p|\mathbf{k}|}\right. \\
&\left. - \frac{p^2(\mathbf{k}^2 - k_4^2) + 2m_\pi^2\mathbf{k}^2}{8p|\mathbf{k}|}\right)\ln a_\pi \\
&- \frac{i\omega_\pi k_4(k_4^2 + \mathbf{k}^2)(k_4^2 + \mathbf{k}^2 + m_\rho^2 - m_\pi^2)}{8p|\mathbf{k}|^3}\ln b_\pi\Bigg]\frac{1}{e^{\beta\omega_\pi} - 1} \\
&+ \frac{1}{\omega_\rho}\Bigg[\frac{(k_4^2 - \mathbf{k}^2)(k_4^2 + \mathbf{k}^2 + m_\pi^2 - m_\rho^2)}{4\mathbf{k}^2} \\
&+ \left(\frac{(k_4^2 - \mathbf{k}^2)\left((k_4^2 + \mathbf{k}^2 + m_\pi^2 - m_\rho^2)^2 - 4\omega_\rho^2 k_4^2\right)}{32p|\mathbf{k}|^3} - \frac{\omega_\rho^2 k_4^2}{2p|\mathbf{k}|}\right. \\
&\left. - \frac{p^2(\mathbf{k}^2 - k_4^2) + 2m_\rho^2\mathbf{k}^2}{8p|\mathbf{k}|}\right)\ln a_\rho \\
&- \frac{i\omega_\rho k_4(k_4^2 + \mathbf{k}^2)(k_4^2 + \mathbf{k}^2 + m_\pi^2 - m_\rho^2)}{8p|\mathbf{k}|^3}\ln b_\rho\Bigg]\frac{1}{e^{\beta\omega_\rho} - 1}\Bigg\}, \tag{2.10}
\end{aligned}$$

$$B = 3\left(\frac{g_{\phi\rho\pi}}{2\pi}\right)^2 \int\limits_0^\infty dp\, p^2 \left\{ \frac{1}{\omega_\pi} \left[\frac{-(3k_4^2 - k^2)(k_4^2 + k^2 + m_\rho^2 - m_\pi^2)}{4k^2} \right.\right.$$

$$- \left(\frac{(3k_4^2 - k^2)\left((k_4^2 + k^2 + m_\rho^2 - m_\pi^2)^2 - 4\omega_\pi^2 k_4^2\right)}{32p|k|^3} - \frac{\omega_\pi^2 k_4^2}{2p|k|} \right.$$

$$\left. - \frac{m_\pi^2 |k|}{4p} - \frac{p(k_4^2 + k^2)}{8|k|} \right) \ln a_\pi$$

$$\left. + \frac{i\omega_\pi k_4(3k_4^2 + k^2)(k_4^2 + k^2 + m_\rho^2 - m_\pi^2)}{8p|k|^3} \ln b_\pi \right] \frac{1}{e^{\beta\omega_\pi} - 1}$$

$$+ \frac{1}{\omega_\rho} \left[\frac{-(3k_4^2 - k^2)(k_4^2 + k^2 + m_\pi^2 - m_\rho^2)}{4k^2} \right.$$

$$- \left(\frac{(3k_4^2 + k^2)\left((k_4^2 + k^2 + m_\pi^2 - m_\rho^2)^2 - 4\omega_\rho^2 k_4^2\right)}{32p|k|^3} \right.$$

$$\left. - \frac{\omega_\rho^2 k_4^2}{2p|k|} - \frac{m_\rho^2 |k|}{4p} - \frac{p(k_4^2 + k^2)}{8|k|} \right) \ln a_\rho$$

$$\left.\left. + \frac{i\omega_\pi k_4(3k_4^2 + k^2)(k_4^2 + k^2 + m_\pi^2 - m_\rho^2)}{8p|k|^3} \ln b_\rho \right] \frac{1}{e^{\beta\omega_\rho} - 1} \right\}, \tag{2.11}$$

and finally,

$$a_\pi = \frac{(k_4^2 + k^2 + m_\rho^2 - m_\pi^2 - 2p|k|)^2 + 4\omega_\pi^2 k_4^2}{(k_4^2 + k^2 + m_\rho^2 - m_\pi^2 + 2p|k|)^2 + 4\omega_\pi^2 k_4^2},$$

$$a_\rho = \frac{(k_4^2 + k^2 + m_\pi^2 - m_\rho^2 - 2p|k|)^2 + 4\omega_\rho^2 k_4^2}{(k_4^2 + k^2 + m_\pi^2 - m_\rho^2 + 2p|k|)^2 + 4\omega_\rho^2 k_4^2},$$

$$b_\pi = \frac{(k_4^2 + k^2 + m_\rho^2 - m_\pi^2)^2 - 4(p|k| + i\omega_\pi k_4)^2}{(k_4^2 + k^2 + m_\rho^2 - m_\pi^2)^2 - 4(p|k| - i\omega_\pi k_4)^2},$$

$$b_\rho = \frac{(k_4^2 + k^2 + m_\pi^2 - m_\rho^2)^2 - 4(p|k| + i\omega_\rho k_4)^2}{(k_4^2 + k^2 + m_\pi^2 - m_\rho^2)^2 - 4(p|k| - i\omega_\rho k_4)^2}, \tag{2.12}$$

where $\omega_\pi = \sqrt{p^2 + m_\pi^2}$ and $\omega_\rho = \sqrt{p^2 + m_\rho^2}$. We have evaluated these components separately and then checked for transversality as required by current conservation.

III. FULL PROPAGATOR

We next let time become real which changes the space-time from Euclidean to Minkowskian. The metric is now $+ - - -$ for $\mu = 0, 1, 2, 3$. We can decompose the self-energy into scalar functions times longitudinal and transverse projection tensors defined to be

$$P_T^{00} = P_T^{0i} = P_T^{i0} = 0,$$
$$P_T^{ij} = \delta^{ij} - k^i k^j / k^2,$$
$$P_L^{\mu\nu} = k^\mu k^\nu / k^2 - g^{\mu\nu} - P_T^{\mu\nu}. \tag{3.1}$$

5

The decomposition reads

$$\Pi^{\mu\nu}(k) = F(k)P_L^{\mu\nu} + G(k)P_T^{\mu\nu}. \tag{3.2}$$

Utilizing this, we have

$$F = -\frac{k^2}{\mathbf{k}^2}\Pi^{44}, \qquad G = A, \tag{3.3}$$

where Π^{44} and A are given by Eqs. (2.7) and (2.10) with $ik_4 = k_0$. Inner-products are again Minkowskian, e.g. $k^2 = k_0^2 - \mathbf{k}^2$. The all-important connection with the full and bare propagator comes next, it is

$$\Pi^{\mu\nu} = (\mathcal{D}^{\mu\nu})^{-1} - (\mathcal{D}_0^{\mu\nu})^{-1}. \tag{3.4}$$

Therefore, the full ϕ-meson propagator can be written as

$$\mathcal{D}^{\mu\nu} = -\frac{P_L^{\mu\nu}}{k^2 - m_\phi^2 - F} - \frac{P_T^{\mu\nu}}{k^2 - m_\phi^2 - G} - \frac{k^\mu k^\nu}{k^2 m_\phi^2}. \tag{3.5}$$

The first two pieces represent the longitudinal and transverse collective excitations of the resonance at finite temperature and in general, are different. To learn just how different they are for $T > 0$ is now a numerical task which will be discussed later.

In the vacuum there is no preferred rest frame and the scalar functions F and G become equal. After dimensional regularization and renormalization we arrive at finite results

$$\begin{aligned}
F_{\text{vac}} = G_{\text{vac}} = \frac{g_{\phi\rho\pi}^2}{16\pi^2}M^2 &\left\{ \frac{-1}{2M^2}\left((m_\rho^2 - m_\pi^2 - M^2)^2 - 4m_\pi^2 M^2\right)\sqrt{\mathcal{R}} \right. \\
&\times \left[\ln\left|\frac{4m_\pi m_\rho/M^2}{\left(1 - \frac{m_\rho^2 - m_\pi^2}{M^2} - \sqrt{\mathcal{R}}\right)\left(1 + \frac{m_\rho^2 - m_\pi^2}{M^2} - \sqrt{\mathcal{R}}\right)}\right| + i\pi\Theta\left(M^2 - (m_\pi + m_\rho)^2\right) \right] \\
&- \frac{1}{2M^4}(m_\rho^2 - m_\pi^2 - M^2)\left[\left(m_\rho^2 - m_\pi^2 - M^2\right)^2 - 6m_\pi^2 M^2\right]\ln\left(\frac{m_\rho}{m_\pi}\right) \\
&\left. + \frac{5}{6}M^2 + \frac{(m_\rho^2 - m_\pi^2)^2}{2M^2} - 2\left(m_\rho^2 + m_\pi^2\right) + C\left(3m_\rho^2 + 3m_\pi^2 - M^2\right) \right\}
\end{aligned} \tag{3.6}$$

where now the radicand is

$$\mathcal{R} = \left(1 - \frac{m_\rho^2 - m_\pi^2}{M^2}\right)^2 - \frac{4m_\pi^2}{M^2}, \tag{3.7}$$

and the invariant mass of the resonance is $M = \sqrt{k^2}$ while its energy is $E = \sqrt{M^2 + \mathbf{k}^2}$ in the rest frame of the hadron gas. We determine the renormalization constant by imposing the physical-mass condition, namely, $\text{Re}\,F_{\text{vac}}(k^2 = m_\phi^2) = 0$. It determines the constant to be

$$C = \frac{1}{\left(3m_\rho^2 + 3m_\pi^2 - m_\phi^2\right)} \left\{ \frac{1}{2m_\phi^2} \left((m_\rho^2 - m_\pi^2 - m_\phi^2)^2 - 4m_\pi^2 m_\phi^2\right) \sqrt{\mathcal{R}'} \right.$$

$$\times \ln \left| \frac{4m_\pi m_\rho / m_\phi^2}{\left(1 - \frac{m_\rho^2 - m_\pi^2}{m_\phi^2} - \sqrt{\mathcal{R}'}\right)\left(1 + \frac{m_\rho^2 - m_\pi^2}{m_\phi^2} - \sqrt{\mathcal{R}'}\right)} \right|$$

$$+ \frac{1}{2m_\phi^4}(m_\rho^2 - m_\pi^2 - m_\phi^2)\left[\left(m_\rho^2 - m_\pi^2 - m_\phi^2\right)^2 - 6m_\pi^2 m_\phi^2\right] \ln\left(\frac{m_\rho}{m_\pi}\right)$$

$$\left. -\frac{5}{6}m_\phi^2 - \frac{(m_\rho^2 - m_\pi^2)^2}{2m_\phi^2} + 2\left(m_\rho^2 + m_\pi^2\right) \right\} \tag{3.8}$$

which use yet a different radicand

$$\mathcal{R}' = \left(1 - \frac{m_\rho^2 - m_\pi^2}{m_\phi^2}\right)^2 - \frac{4m_\pi^2}{m_\phi^2}. \tag{3.9}$$

At finite temperature the functions F and G have—in addition to the vacuum piece—a piece due to the matter $F = F_{\text{vac}} + F_{\text{mat}}$ and $G = G_{\text{vac}} + G_{\text{mat}}$, where

$$F_{\text{mat}} = -3\frac{g_{\phi\rho\pi}^2}{4\pi^2}\frac{M^2}{k^2} \int_0^\infty dp\, p^2 \left\{ \frac{1}{\omega_\pi}\left[\frac{(M^2 - m_\rho^2 + m_\pi^2)}{2} \right.\right.$$

$$+ \frac{-4\omega_\pi^2 E^2 + 4p^2 k^2 - (M^2 - m_\rho^2 + m_\pi^2)^2}{16p|k|}[\ln|a_\pi| + i\pi\mathcal{B}_\pi]$$

$$\left. + \frac{\omega_\pi E(-M^2 + m_\rho^2 - m_\pi^2)}{4p|k|}[\ln|b_\pi| - i\pi\mathcal{B}_\pi]\right] \frac{1}{e^{\beta\omega_\pi} - 1}$$

$$+ \frac{1}{\omega_\rho}\left[\frac{(M^2 - m_\pi^2 + m_\rho^2)}{2} \right.$$

$$+ \frac{-4\omega_\rho^2 E^2 + 4p^2 k^2 - (M^2 - m_\pi^2 + m_\rho^2)^2}{16p|k|}[\ln|a_\rho| + i\pi\mathcal{B}_\rho]$$

$$\left.\left. + \frac{\omega_\rho E(-M^2 + m_\pi^2 - m_\rho^2)}{4p|k|}[\ln|b_\rho| - i\pi\mathcal{B}_\rho]\right] \frac{1}{e^{\beta\omega_\rho} - 1}\right\}, \tag{3.10}$$

$$G_{\text{mat}} = -3\frac{g_{\phi\rho\pi}^2}{4\pi^2} \int_0^\infty dp\, p^2 \left\{ \frac{1}{\omega_\pi}\left[\frac{-(E^2 + k^2)(M^2 - m_\rho^2 + m_\pi^2)}{4k^2} \right.\right.$$

$$+ \left(\frac{(E^2 + k^2)\left((M^2 - m_\rho^2 + m_\pi^2)^2 + 4\omega_\pi^2 E^2\right)}{32p|k|^3} - \frac{\omega_\pi^2 E^2}{2p|k|} \right.$$

$$\left. + \frac{p^2(E^2 + k^2) + 2m_\pi^2 k^2}{8p|k|} \right) [\ln|a_\pi| + i\pi\mathcal{B}_\pi]$$

$$+ \frac{\omega_\pi E M^2(M^2 - m_\rho^2 + m_\pi^2)}{8p|k|^3}[\ln|b_\pi| - i\pi\mathcal{B}_\pi]\right] \frac{1}{e^{\beta\omega_\pi} - 1}$$

$$+\frac{1}{\omega_\rho}\left[\frac{-(E^2+k^2)(M^2-m_\pi^2+m_\rho^2)}{4k^2}\right.$$

$$+\left(\frac{(E^2+k^2)\left((M^2-m_\pi^2+m_\rho^2)^2+4\omega_\rho^2 E^2\right)}{32p|k|^3}-\frac{\omega_\rho^2 E^2}{2p|k|}\right.$$

$$\left.+\frac{p^2(E^2+k^2)+2m_\rho^2 k^2}{8p|k|}\right)[\ln|a_\rho|+i\pi\mathcal{B}_\rho]$$

$$\left.+\frac{\omega_\rho E M^2(M^2-m_\pi^2+m_\rho^2)}{8p|k|^3}[\ln|b_\rho|-i\pi\mathcal{B}_\rho]\right]\frac{1}{e^{\beta\omega_\rho}-1}\Bigg\},\tag{3.11}$$

and

$$\mathcal{B}_\pi=\begin{cases}1 & \text{if } \mu_{\text{low}}\leq 2p\leq\mu_{\text{high}}\\ 0 & \text{otherwise}\end{cases}\tag{3.12}$$

$$\mathcal{B}_\rho=\begin{cases}1 & \text{if } \nu_{\text{low}}\leq 2p\leq\nu_{\text{high}}\\ 0 & \text{otherwise}\end{cases}\tag{3.13}$$

where

$$\mu_{\text{low}}=\left|E\sqrt{\left(1+\frac{m_\pi^2-m_\rho^2}{M^2}\right)^2-\frac{4m_\pi^2}{M^2}}-|k|\left(1+\frac{m_\pi^2-m_\rho^2}{M^2}\right)\right|$$

$$\mu_{\text{high}}=\left|E\sqrt{\left(1+\frac{m_\pi^2-m_\rho^2}{M^2}\right)^2-\frac{4m_\pi^2}{M^2}}+|k|\left(1+\frac{m_\pi^2-m_\rho^2}{M^2}\right)\right|\tag{3.14}$$

and

$$\nu_{\text{low}}=\left|E\sqrt{\left(1+\frac{m_\rho^2-m_\pi^2}{M^2}\right)^2-\frac{4m_\rho^2}{M^2}}-|k|\left(1+\frac{m_\rho^2-m_\pi^2}{M^2}\right)\right|$$

$$\nu_{\text{high}}=\left|E\sqrt{\left(1+\frac{m_\rho^2-m_\pi^2}{M^2}\right)^2-\frac{4m_\rho^2}{M^2}}+|k|\left(1+\frac{m_\rho^2-m_\pi^2}{M^2}\right)\right|.\tag{3.15}$$

It is difficult to do little else with these expressions except numerical analyses.

A. Effective widths, masses and dispersion relations

Decays are of course observable. In the Particle Data Group tables one has experimental values for free-space partial and total decay widths. They provide calibration for our calculation since the partial decay width can be related to the imaginary part of F (or G, since they are the same in vacuum) as follows

$$\Gamma_{\phi\to\pi\rho}=-\frac{1}{m_\phi}\text{Im}\,F_{\text{vac}}(k^2=m_\phi^2).\tag{3.16}$$

This uniquely determines the value of $g_{\phi\rho\pi}$. It is indeed quite reassuring that the decay width calculated this way is precisely what one gets from an S-matrix approach for the net decay into a $\pi\rho$ combination, namely,

$$\Gamma_{\phi\to\rho\pi} = \frac{1}{24}\left(\frac{m_\phi^2 g_{\phi\pi}^2}{4\pi}\right)\frac{1}{m_\phi^5}\left[\left(m_\rho^2 - m_\pi^2 - m_\phi^2\right)^2 - 4m_\pi^2 m_\phi^2\right]^{3/2}. \tag{3.17}$$

Note that as we are using it, $g_{\phi\rho\pi}$ has units of inverse mass. The relevant formula for the two-kaon decay is

$$\Gamma_{\phi\to KK} = \frac{2}{3}\left(\frac{g_{\phi KK}^2}{4\pi}\right)\frac{1}{m_\phi^2}\left[\frac{m_\phi^2}{4} - m_K^2\right]^{3/2}. \tag{3.18}$$

Throughout this work we have used $m_\pi = 139.6$ MeV, $m_K = 493.6$ MeV, $m_\rho = 768.1$ MeV, $m_\phi = 1019.4$ MeV, the full width $\Gamma_\phi = 4.43$ MeV and partial widths $\Gamma_{\phi\to KK}/\Gamma_\phi = 49.1\%$ and $\Gamma_{\phi\to\rho\pi}/\Gamma_\phi = 12.9\%$. Equation (3.17) determines $m_\phi^2 g_{\phi\rho\pi}^2/4\pi = 0.29$, while Eq. (3.18) determines $g_{\phi KK}^2/4\pi = 1.65$.

In Figs. 2 and 3 we show $-F_{\mathrm{I}}$ and using $k = 0.05$ GeV/c and $k = 0.75$ GeV/c. In each plot, three curves are shown. Solid, dashed and dotted curves correspond to temperatures $T = 0$, 100 and 200 MeV, respectively. Below the two-kaon threshold the $\pi\rho$ contribution stands alone and is noticeably affected by temperature. The imaginary part of G behaves almost identically to F, so we do not show it. Equation (3.16) also determines an effective width for nonzero temperatures with the replacement

$$F_{\mathrm{vac}} \to F = F_{\mathrm{vac}} + F_{\mathrm{mat}} \tag{3.19}$$

This effective width is now dependent not only on the invariant mass of the resonance, but separately on its three-momentum. It is also polarization dependent since instead of F we might have used G. In practice, this difference is not noticeable. So using a small value of momentum we plot the effective widths in Fig. 4. The $\pi\rho$ channel nearly double its (zero temperature) value at $T = 200$ MeV. Since the two-kaon channel is larger and is affected less by temperature, the sum of the two channels changes only modestly. The value for the width of the sum of both channels goes from 2.75, to 2.84, to 3.06 and finally, to 3.39 MeV at temperatures 0, 100, 150 and 200 MeV, respectively.

An effective mass can be determined from the pole of the propagator. It shifts somewhat due to the presence of matter since F and G have nonzero real parts. These parts are in general different thereby introducing a *polarization dependence*. But in the limit $k \to 0$, F and G become equal and one can speak of an effective mass. Formally, it is the value of k_0 which satisfies

$$k_0^2 - m_\phi^2 - F_{\mathrm{R}}(k_0, |\boldsymbol{k}| \to 0, T) = 0. \tag{3.20}$$

We extract it from our numerical results. In Fig. 5 we show this effective mass minus the vacuum mass as a function of temperature: It rises with rising temperature. At $T = 200$ MeV, the effective mass calculated this way increases by ~ 4 MeV. For finite three-momentum the situation is more complicated so we show the K^+K^- and the $\pi\rho$ contributions to the real part of the function F at two different momenta in Figs. 6 and 7. The $\pi\rho$ results

are distinquishable from the two-kaon results since they extend below the two-kaon threshold. For each, three curves are shown: $T = 0$, 150 and 200 MeV temperature correspond to solid, dashed and dotted lines, respectively. The noteworthy features are these. The $\pi\rho$ contribution is increased at finite temperature for masses ranging from threshold to roughly 1.3–1.6 GeV (depending on the temperature and momentum) where it becomes reduced with finite temperature. Temperature effects are quite small here. Kaon contributions are strictly increased at finite temperature for all masses. These increases and reductions have competing effects on the ϕ effective mass.

Since F and G are (very) slightly different, a notion more general than effective mass is needed. So next we consider the relationship between energy and momentum for each polarization, i.e. dispersion. Evaluation of the dispersions requires us to find solutions to

$$k_0^2 = \mathbf{k}^2 + m_\phi^2 + F_{\mathrm{R}}(k_0, |\mathbf{k}|, T),$$
$$k_0^2 = \mathbf{k}^2 + m_\phi^2 + G_{\mathrm{R}}(k_0, |\mathbf{k}|, T),$$
(3.21)

for given values of $|\mathbf{k}|$ and T. They determine the longitudinal and transverse dispersion relations ω_k^{L} and ω_k^{T}. We present them in Figs. 8 and 9 wherein the solid curves are for $T = 0$, while dashed and dotted curves correspond to $T = 150$ and 200 MeV results, respectively. The effect is small but the direction of it is quite clear. We see an increase in the effective mass with temperature. The transverse polarization effects in Fig. 9 are just slightly greater.

B. thermal dilepton emission rates

The electron-positron production rate has been shown to be related to the imaginary part of the retarded photon self-energy [5]. Since vector-meson dominance suggests that a virtual photon converts first to a neutral vector meson which then couples to other hadrons, the photon self-energy can be simply related to the imaginary part of the vector meson propagator. Derivational details of this equivalence and the formulas can be found in Refs. [11]–[14] and [5]. We merely state the formula for the production rate for arbitrary momentum configurations proceeding through the ϕ-meson

$$E_+ E_- \frac{dR}{d^3 p_+ d^3 p_-} = \frac{1}{(2\pi)^6} \frac{e^4}{\tilde{g}_\phi^2} \frac{m_\phi^4}{M^4} \left\{ \left[q^2 - (q \cdot \hat{k})^2\right] \frac{-F_{\mathrm{I}}}{\left(M^2 - m_\phi^2 - F_{\mathrm{R}}\right)^2 + F_{\mathrm{I}}^2} \right.$$
$$\left. + \left[2M^2 - q^2 + (q \cdot \hat{k})^2\right] \frac{-G_{\mathrm{I}}}{\left(M^2 - m_\phi^2 - G_{\mathrm{R}}\right)^2 + G_{\mathrm{I}}^2} \right\} \frac{1}{e^{\beta E} - 1}$$
(3.22)

where for convenience we have used $q^\mu = p_+^\mu - p_-^\mu$ and momentum conservation forces $k^\mu = p_+^\mu + p_-^\mu$. The rate for $e^+ e^-$ production below the two-kaon threshold is obtained from Eq. (3.22) with $\tilde{g}_\phi$ adjusted to give the right $\phi \to e^+ e^-$ decay. For invariant masses above threshold, one adjusts $\tilde{g}_\phi$ to achieve continuity in the rate at $M = 2m_K$. Here the real and imaginary parts of F and G have contributions from both kaon-loop and $\pi\rho$ loop diagrams. Though we do not show them, the rates for the individual channels are (branching ratio) fractions of this total rate. For example,

$$E_+ E_- \frac{dR_{\pi\rho \to \phi \to e^+ e^-}}{d^3 p_+ d^3 p_-} = \left(\frac{F_I^{\pi\rho}}{F_I^{\pi\rho} + F_I^{K^+ K^-}} \right) E_+ E_- \frac{dR_{\text{total}}}{d^3 p_+ d^3 p_-} \qquad (3.23)$$

for longitudinal polarizations. Then the same expression is used with the function F replaced by G for transverse polarizations.

As mentioned several times already, dielectron spectra depend on polarization. For example,

$$q^2 - (q \cdot \hat{k})^2 = \begin{cases} M^2 & \text{if } q \perp k \\ 0 & \text{if } q \parallel k \end{cases}$$

$$2M^2 - q^2 + (q \cdot \hat{k})^2 = \begin{cases} M^2 & \text{if } q \perp k \\ 2M^2 & \text{if } q \parallel k \end{cases} \qquad (3.24)$$

While at first this seems like a potentially useful tool, we find it is a tiny effect for these processes. Shown in Figs. 10 and 11 are the (sum of the two) rates of dielectron production at two different total momenta $k = 0.05$ and 0.75 GeV/c. The solid curve uses a temperature independent form factor and the longitudinal and transverse contributions are presented as dashed and dotted lines, respectively. Keeping with the above statement about polarizations, we note that though they are truly distinct especially at higher momentum, one probably cannot expect to utilize this difference in experiment. Another way to think of the effective mass is that it is the average invariant mass of all back-to-back kinematically allowed configurations for the dileptons. If one imagines doing such an average in Fig. 10, one can see the rise. Both the kaons' and the $\pi\rho$'s contributions tend to raise the effective mass.

IV. CONCLUSIONS

It is not possible to overstate the importance of understanding hadronic processes whitin hot matter. As the temperature rises above say, 150 MeV and approaches 200 MeV, hadronic interactions may well deviate drastically from vacuum behavior. These modifications are quite important both from theoretical and experimental points of view. Open questions abound with regard to the approach to chiral symmetry restoration and deconfinement phase transition. A solid understanding of hadronic physics is essential for making progress in this direction. We have studied how temperature affects properties of the ϕ-meson. By evaluating a new contribution to the one-loop self-energy, we have improved estimates for the decay width, dispersion relations or effective mass, and finally, for the rate of dielectron production with invariant masses near the ϕ.

We have learned that within this type of modelling for the relevant hadronic degrees of freedom and their (strong) interaction, the effective mass of the ϕ-meson is nearly temperature independent below ~ 50 MeV. Above this, it shows slight increase: It rises by 0.42, 1.55, and 4.59 MeV at temperatures 100, 150 and 200 MeV, respectively. This rise is mostly due to the kaon contributions, although the effect of the $\pi\rho$ channel is to move the mass in the same direction. These results for the effective mass contrast with some QCD sum-rule calculations at finite (temperature and) density [15], where a large decrease of the ϕ-meson mass at $T \neq 0$, e.g. ~ 100 MeV reduction at $T = 175$ MeV. However, it is vital in such calculations to treat the spectral-function side of the sum rule consistently with the change of

the condensate appearing in the operator product expansion. Moreover, the absence of the $O(T^2)$ mass shift is quite a general result on the basis of chiral symmetry [16,17]. Koike [18] further points out in the context of QCD sum rules for the vector mesons at finite density (in nuclear matter) that the medium (density) dependent part of the correlation function has to be identified from the point of view of the forward current-nucleon scattering amplitude. This statement also applies to the finite-T sum rule for the ϕ-meson [19]. In support of approaches like ours we wish to stress here its virtues of self–consistency: the thermal modifications of the real and of the imaginary parts of the ϕ self–energy are computed simultaneously, not just one or the other. This has considerable appeal for the point of view of theory.

The partial decay width into the $\pi\rho$ channel is the most affected by temperature. Since it is smaller than the kaon channel to begin with, the net result for the width's modification is also modest. At 150 MeV temperature, the width increases by 11% and at 200 MeV temperature it increases by 23% as compared to its vacuum value. The thermal rate of dielectron production near the ϕ mass was shown to be altered accordingly. Polarization effects are insignificantly small.

While our study answers some questions about temperature's affect on properties of the ϕ-meson, it does not address some potentially important issues. In the context of a loop expansion of the photon self–energy, collisional broadening effects on the dilepton spectrum are of two–loop order, beyond the present calculation. However, those have recently been estimated [20]. A consistent incorporation of such contributions in our self–consistent framework is desirable and considered. Probably the next-most-important idea to incorporate into this calculation is a modified pion dispersion relation. Pion properties are probably also modified at such high temperatures and it is important to see how sensitive other hadrons' properties are to such things. There is also the question of finite chemical potentials. We have neglected it, but inclusion of a nonzero μ_π is rather straightforward. These activities are planned.

ACKNOWLEDGEMENTS

REFERENCES

* electronic address: haglin@theo03.nscl.msu.edu

** electronic address: gale@physics.mcgill.ca

[1] C. DeTar, Phys. Rev. D **32**, 276 (1985); C. DeTar and J. Kogut, *ibid.* **36**, 2828 (1987).

[2] S. Gottlieb *et al.*, Phys. Rev. Lett. **59**, 347 (1987).

[3] M. Dey, V. L. Eletsky, and B. L. Ioffe, Phys. Lett. B **252**, 620 (1990).

[4] R. Furnstahl, T. Hatsuda, and Su H. Lee, Phys. Rev. D **42**, 1744 (1990); T. Hatsuda, Y. Koike, and Su. H. Lee, Nucl. Phys. **B394**, 221 (1993); Phys. Rev. D **47**, 1225 (1993).

[5] C. Gale and J. Kapusta, Nucl. Phys. **B357**, 65 (1991).

[6] C. Song, Phys. Rev. D **48**, 1375 (1993).

[7] C. Gale and P. Lichard, Phys. Rev. D **49**, 3338 (1994).

[8] D. Lissauer and E. V. Shuryak, Phys. Lett. B **253**, 15 (1991).

[9] U.-G. Meißner, Phys. Rep. **161**, 215 (1988).

[10] P. Ramond, *Field Theory: A Modern Primer* (Addison-Wesley Publishing Company, Inc., 1989).

[11] E. L. Feinberg, Nuovo Cimento **34A**, 391 (1976).

[12] L. D. McLerran and T. Toimela, Phys. Rev. D **31**, 545 (1985).

[13] C. M. Ko, L. H. Xia and P. J. Siemens, Phys. Lett. B **231**, 16 (1989).

[14] H. A. Weldon, Phys. Rev. D **42**, 2384 (1990).

[15] M. Asakawa and C. M. Ko, Texas A & M University preprint, (1992).

[16] V. L. Eletsky and B. L. Ioffe, Phys. Rev. D **47**, 3083 (1993).

[17] Y. Koike, Phys. Rev. D **48**, 2313 (1993).

[18] Y. Koike, NSCL at Michigan State University report no. MSUCL-898 (1993).

[19] Y. Koike, private communication.

[20] C. M. Ko and D. Seibert, preprint CERN-TH-7037-93, Dec 1993.

FIGURES

FIG. 1. Diagrams that contribute to the one-loop ϕ self-energy. The kaon bubble and tadpole are shown in (a) and (b) where the dotted circles represent kaons, while (c) shows the $\pi\rho$ loop.

FIG. 2. The imaginary part of the function F at three-momentum $k = 0.05$ GeV/c as it depends on the invariant mass. The solid curve is the vacuum (T=0) contribution, the dashed and dotted curves correspond to $T = 100$ and 200 MeV, respectively.

FIG. 3. Same as in Fig. 2 except a higher three-momentum of $k = 0.75$ GeV/c.

FIG. 4. Partial decay widths as a function of temperature.

FIG. 5. The effective mass minus the vacuum mass $m_\phi^{\text{eff}} - m_\phi^{\text{vac}}$ versus temperature.

FIG. 6. The real part of F at fixed three-momentum $k = 0.05$ GeV/c as a function of the invariant mass. Kaon contributions correspond to the three curves that begin at the $2m_K$ threshold as indicated. The $\pi\rho$ contributions are the three other curves on which temperature has less affect.

FIG. 7. The same as Fig. 6 with momentum $k = 0.75$ GeV/c.

FIG. 8. Dispersion relation for longitudinally polarized ϕ-mesons at zero (solid curve) and finite temperature (dashed curve T=150 MeV and dotted curve T= 200 MeV).

FIG. 9. Same as Fig. 8 except for transversely polarized ϕ-mesons.

FIG. 10. Dielectron production rate for invariant masses near m_ϕ from the sum of $K^+K^- \rightarrow \phi \rightarrow e^+e^-$ and $\rho\pi \rightarrow \phi \rightarrow e^+e^-$. The solid curve uses a T-independent form factor, whereas the dashed curve is for longitudinal polarizations and the dotted curve is for transverse polarizations. The value of three-momentum and temperature are $k = 0.05$ GeV/c and 200 MeV.
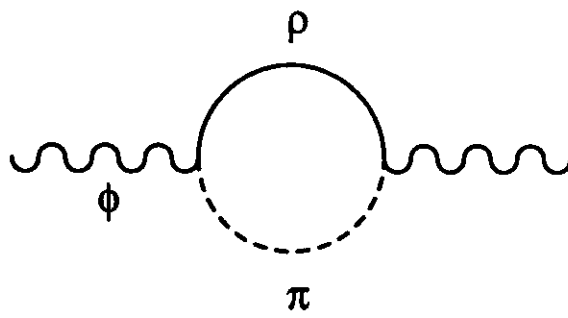
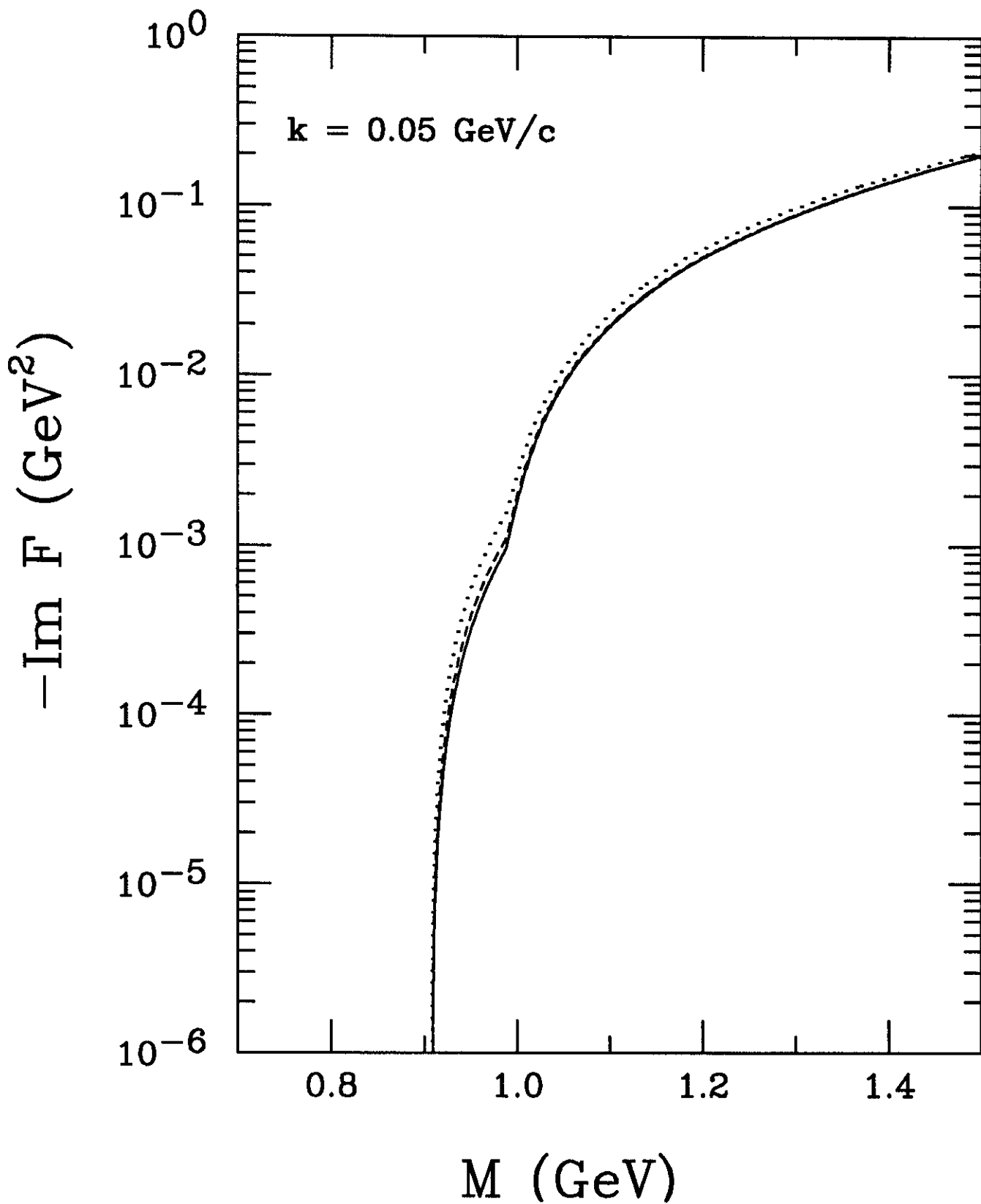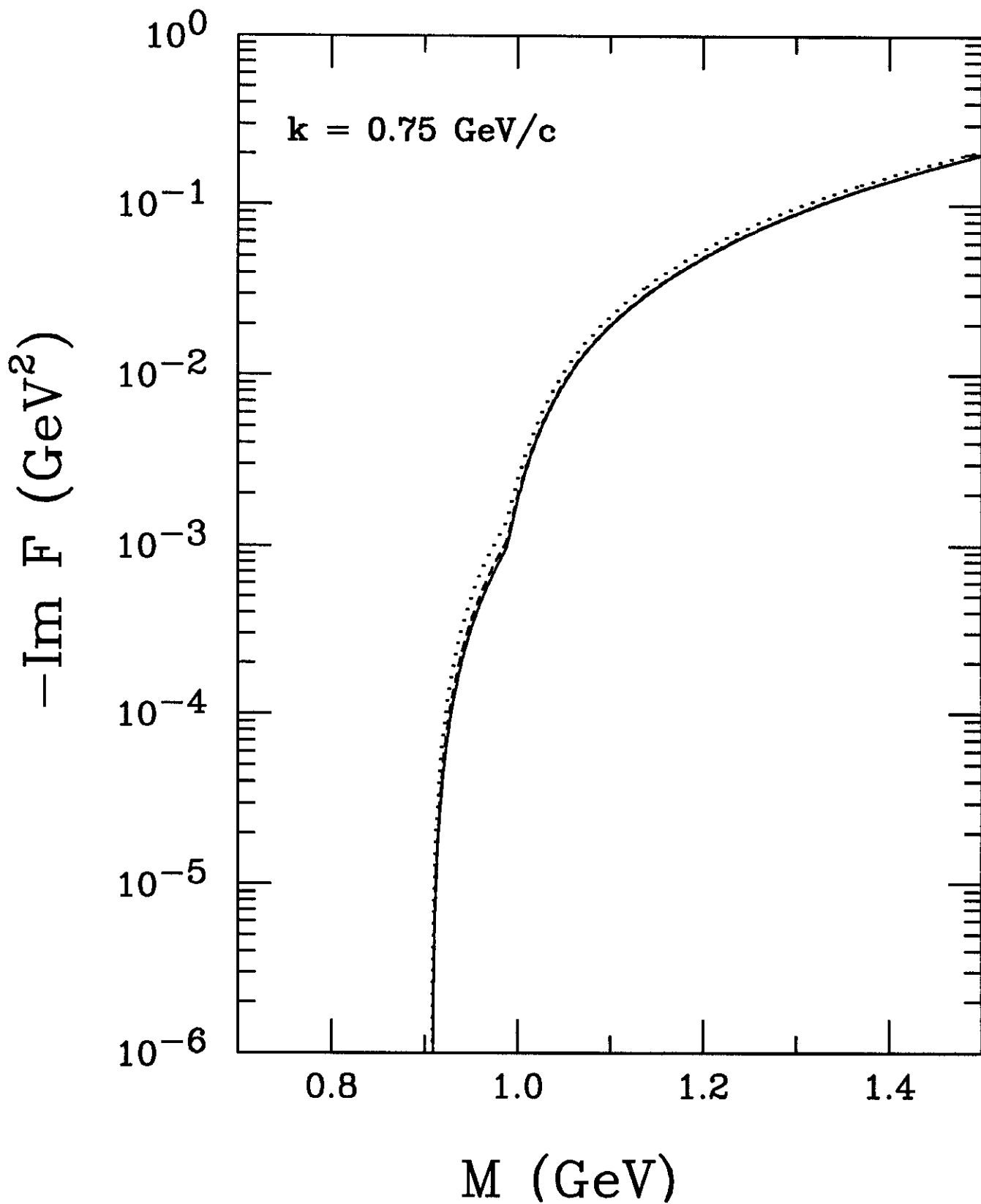FIG. 11. Same as Fig. 10 except momentum $k = 0.75$ GeV/c.

K

φ

K

(a)

(b)

ρ
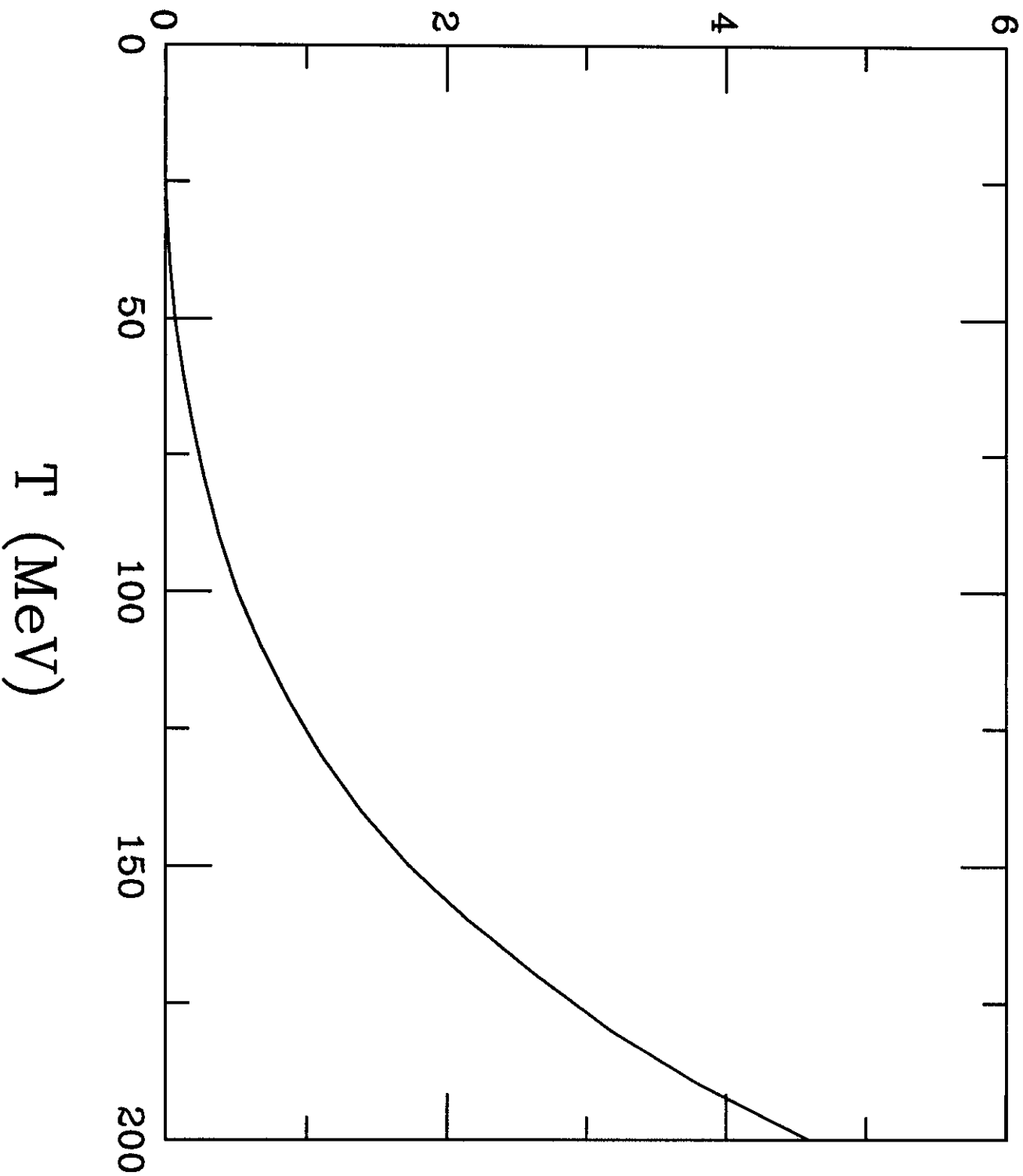
φ

π

(c)

Figure 1

$k = 0.05$ GeV/c

Figure 2

k = 0.75 GeV/c

Figure 3

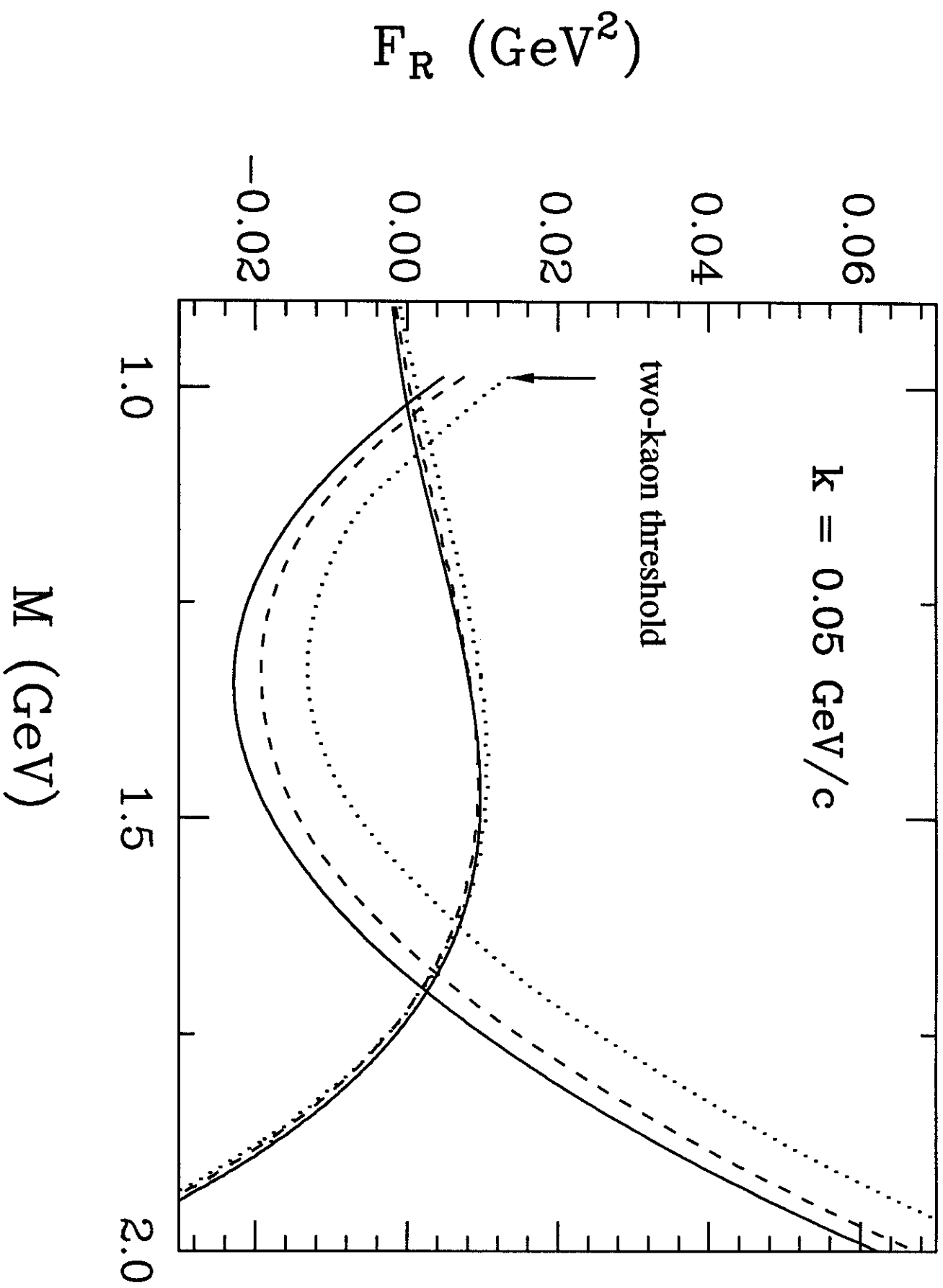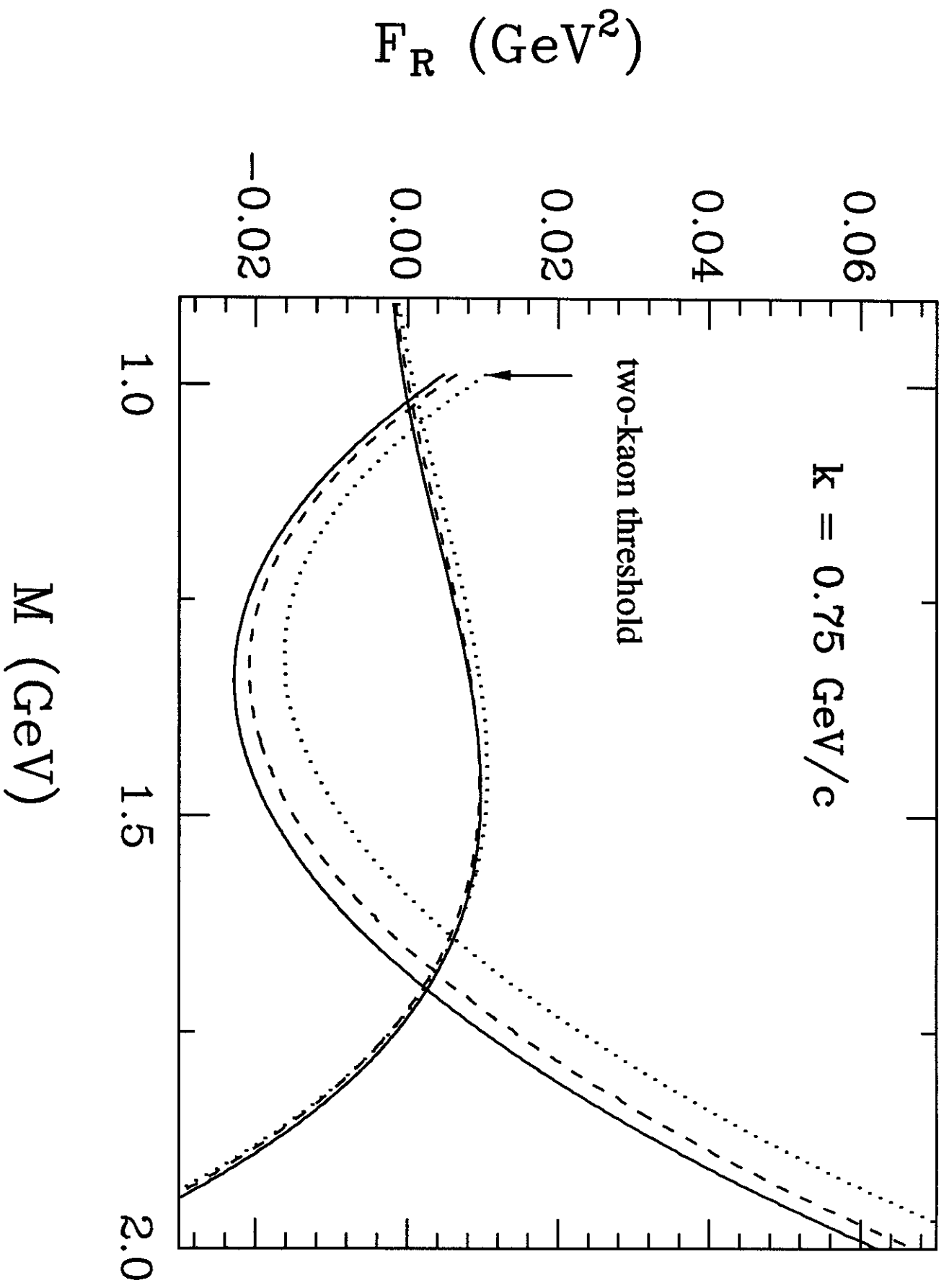Figure 4

Figure 5

Figure 6

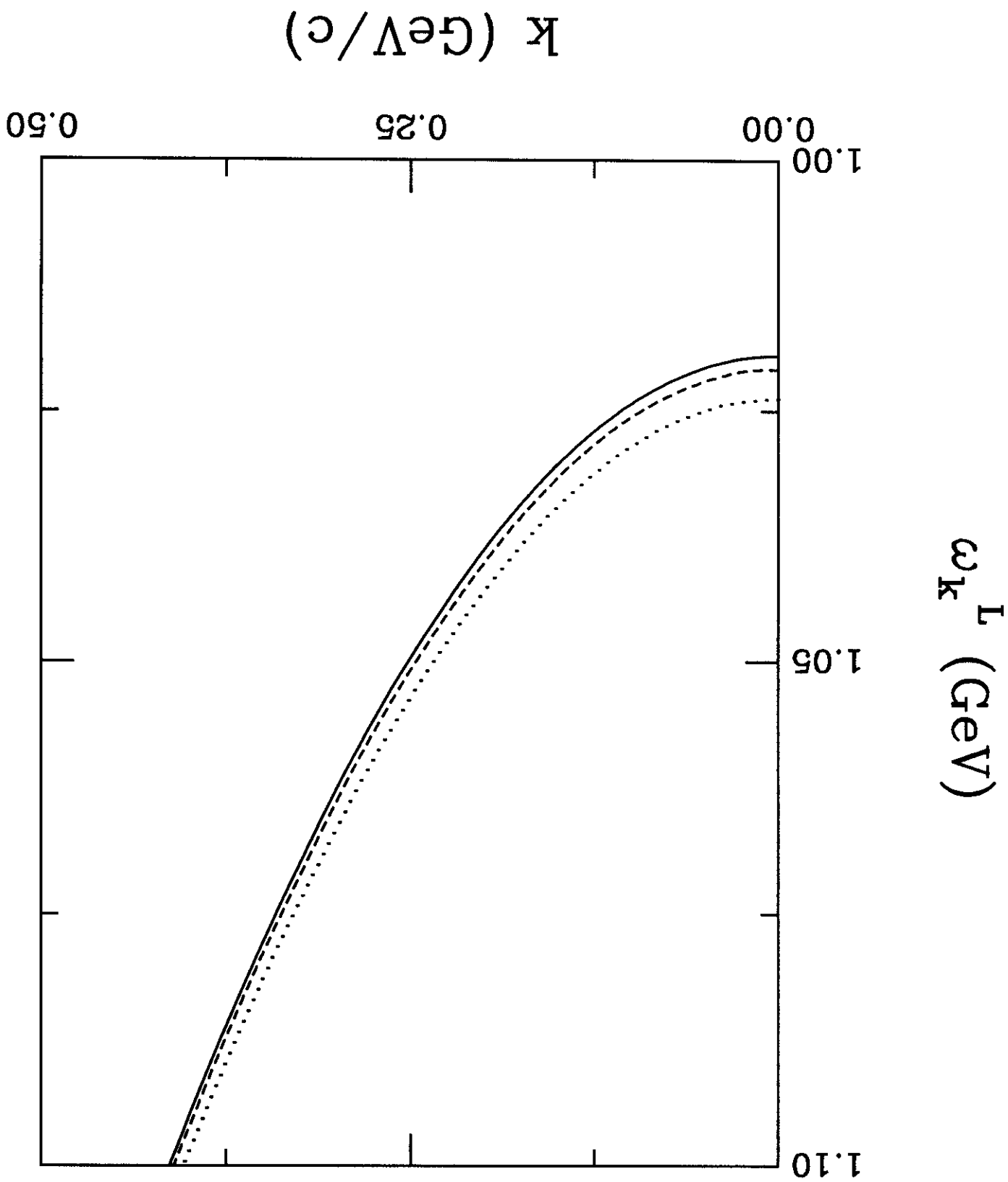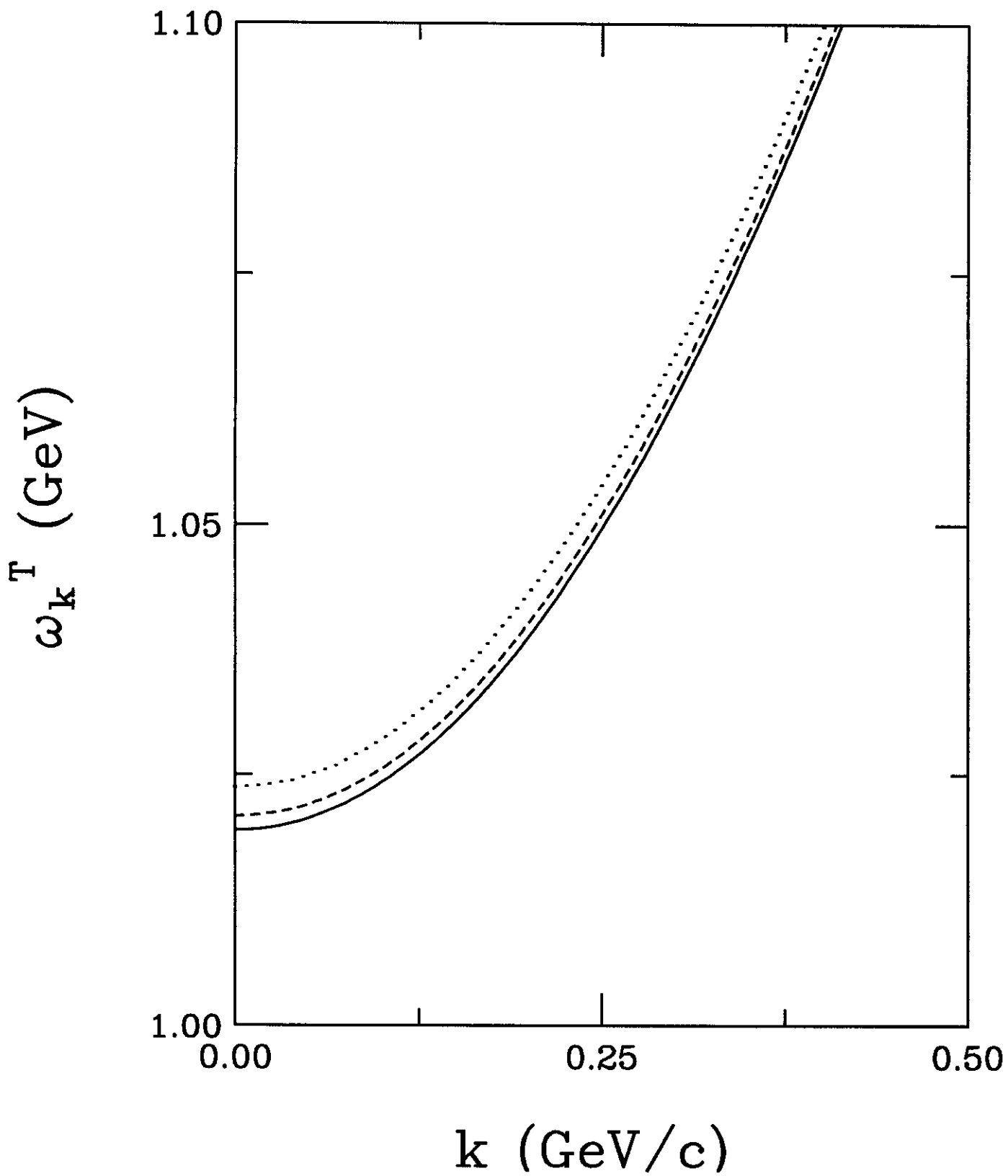F_R (GeV^2)

M (GeV)

k = 0.75 GeV/c

two-kaon threshold
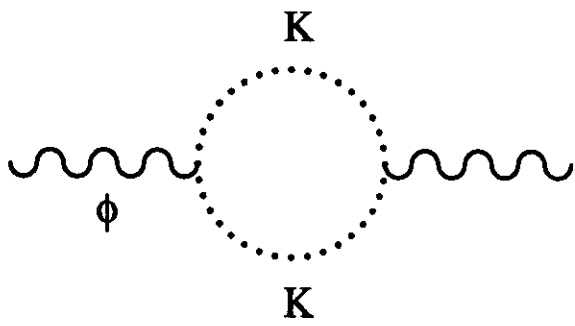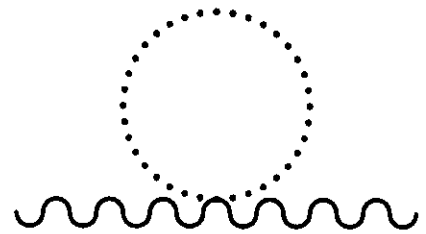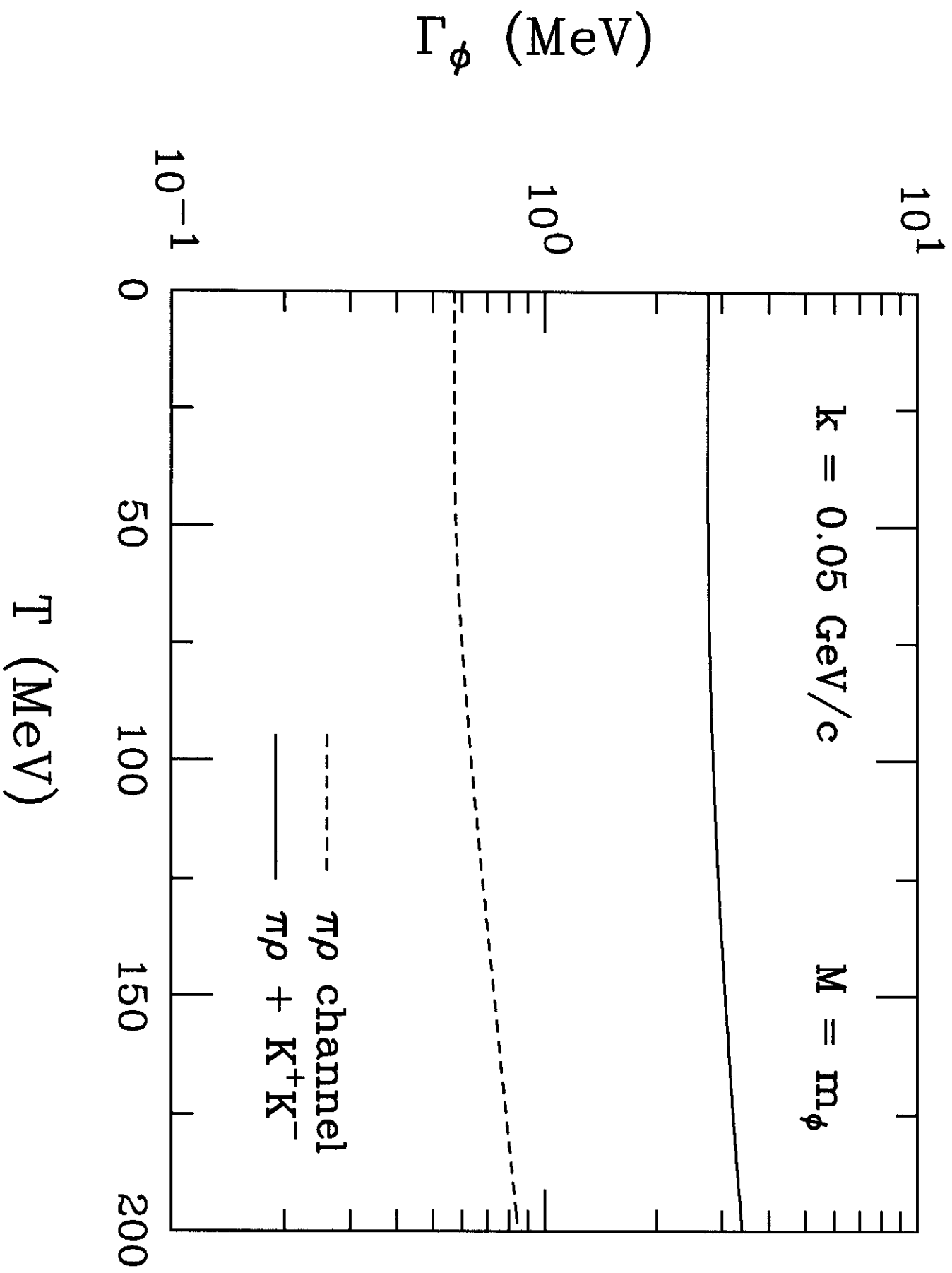
Figure 7

Figure 8

Figure 9

Figure 10

Figure 11